biophysica

MDPI

Article

Physicochemical Characterization of the Catalytic Unit of Hammerhead Ribozyme and Its Relationship with the Catalytic Activity

Yoshiyuki Tanaka [1,*], Daichi Yamanaka [2], Saori Morioka [1], Taishi Yamaguchi [1], Masayuki Morikawa [1], Takashi S. Kodama [3], Vladimír Sychrovský [4,5], Chojiro Kojima [3,6] and Yoshikazu Hattori [1,7]

1 Laboratory of Analytical Chemistry, Department of Pharmaceutical Sciences, Tokushima Bunri University, 180 Nishihama-Boji, Yamashiro-cho, Tokushima 770-8514, Japan
2 Graduate School of Pharmaceutical Sciences, Tohoku University, Sendai 980-8578, Japan
3 Institute for Protein Research, Osaka University, Yamadaoka 3-2, Suita 565-0871, Japan
4 Institute of Organic Chemistry and Biochemistry, Czech Academy of Sciences, Flemingovo náměstí 542/2, 166 10 Praha, Czech Republic
5 Department of Electrotechnology, Faculty of Electrical Engineering, Czech Technical University, Technická 2, 166 00 Praha, Czech Republic
6 Graduate School of Engineering Science, Yokohama National University, Hodogaya-ku, Yokohama 240-8501, Japan
7 Institute of Advanced Medical Sciences, Tokushima University, Kuramoto-cho 3-18-15, Tokushima 770-8503, Japan
* Correspondence: tanakay@ph.bunri-u.ac.jp

Abstract: The catalytic mechanism of hammerhead ribozymes (HHRzs) attracted great attention in relation to the chemical origin of life. However, the basicity (pK_a) of the catalytic sites of HHRzs has not been studied so far. As a result, the investigation of the currently assumed mechanism from an experimentally derived pK_a value has been impossible. In HHRzs, there exists a highly functionalized structural unit (A9-G10.1 site) with a catalytic residue (G12) for the nucleophile activation and metal ion-binding residue (G10.1). As inferred from this fact, there might be a possibility that HHRzs may utilize specific functions of the A9-G10.1 motif for the catalytic reaction. Therefore, here we studied the basicity of G12/G10.1-corresponding residues using RNA duplexes including the A9-G10.1 motif without other conserved residues of HHRzs. From the pH-titration experiments with NMR spectra, we have obtained the intrinsic basicity of the G12/G10.1-corresponding residues in the motif, with pK_a > 11.5 (N1 of G12) and pK_a 4.5 (N7 of G10.1) for the first time. Based on the derived irregular basicity, their correlation with a catalytic activity and a metal affinity were investigated. In total, the derived thermodynamic properties are an intrinsic nature of the exclusive catalytic unit of HHRzs, which will be an outstanding pivot point for the mechanistic analyses.

Keywords: hammerhead ribozyme; mechanism; pK_a; pH-titration; NMR spectroscopy; G12; G10.1

Citation: Tanaka, Y.; Yamanaka, D.; Morioka, S.; Yamaguchi, T.; Morikawa, M.; Kodama, T.S.; Sychrovský, V.; Kojima, C.; Hattori, Y. Physicochemical Characterization of the Catalytic Unit of Hammerhead Ribozyme and Its Relationship with the Catalytic Activity. *Biophysica* **2022**, *2*, 221–239. https://doi.org/10.3390/biophysica2030022

Academic Editors: Attila Borics and Danilo Milardi

Received: 29 July 2022
Accepted: 23 August 2022
Published: 25 August 2022

1. Introduction

The discovery of a catalytic RNA [1,2] such as the hammerhead ribozyme (HHRz) [3–8] stimulated research on the chemical origin of life. Accordingly, HHRzs are a suitable candidate to study one of such topics, namely, how catalytic RNAs can promote chemical reactions (mechanistic studies). Through the mechanistic studies of HHRzs, there have been several breakthroughs. For example, the discovery of HHRzs with peripheral loop–loop interaction (the extended HHRz or the full-length HHRz) [9–14] advanced the understanding of the catalytic mechanism; the loop–loop interaction was found to activate full-length HHRzs (Figure 1) [15–19]. The crystal structure of the full-length HHRz [20–25] revealed a possible active conformation that was consistent with the biochemical experiments [26–28].

Consequently, the reaction mechanism of HHRzs has been discussed on the basis of the structural background [20–25,28–32].

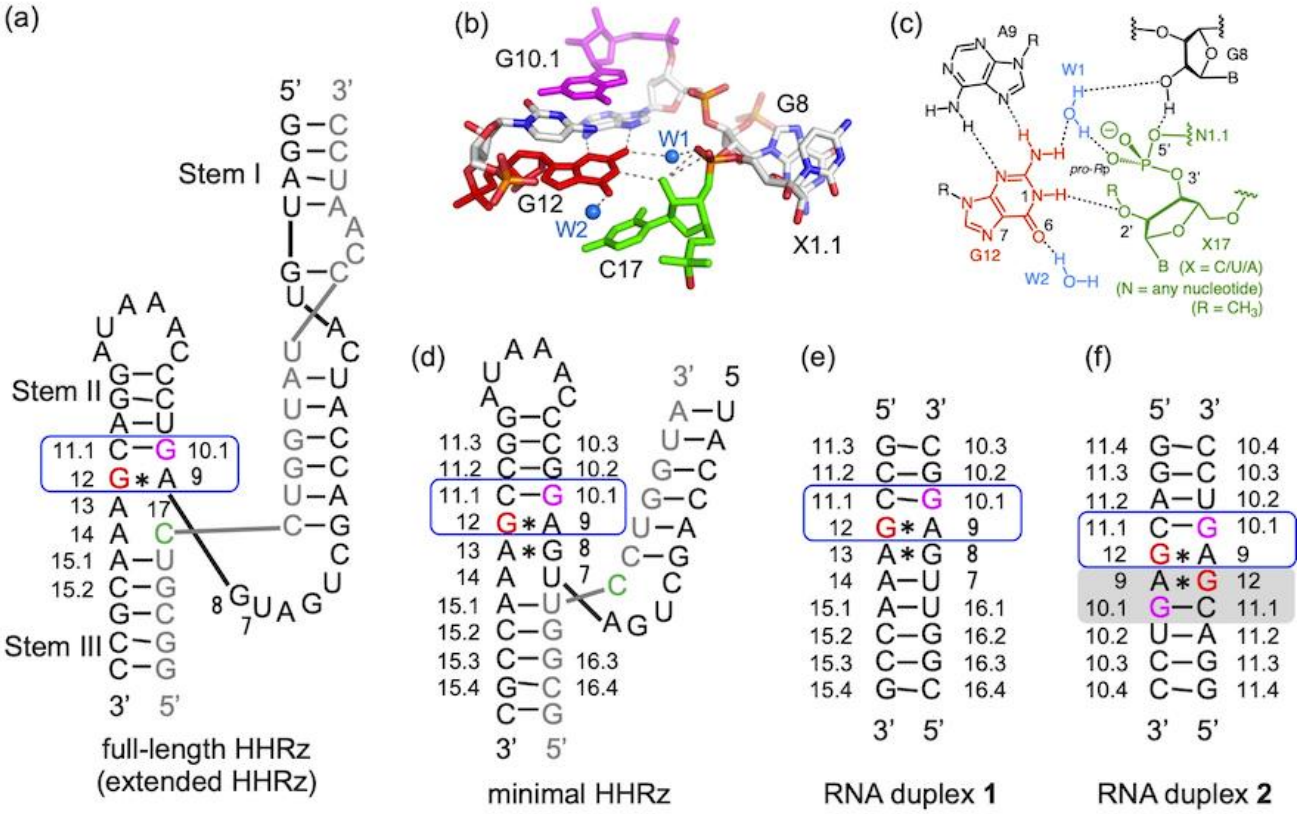

Figure 1. Summary of hammerhead ribozyme (HHRz). (**a**) Secondary structure and sequence of full-length HHRz (extended HHRz) from Schistosoma mansoni. (**b**) Crystal structure (PDB ID: 2OEU [21]) of the catalytic unit (metal ion-binding motif), which would activate the deprotonation of 2′-OH(C17) (X = C in Schistosoma mansoni). Names of the catalytically important residues are shown in the panel, and hydrogen bonds are depicted as broken lines. Methyl groups on the O2′(C17) are omitted for clarity, and the broken lines between O2′(C17) and *pro-*R_P/*pro-*S_P oxygen atoms represent the putative hydrogen bonds for the native 2′-OH form. W1 and W2 are the crystallographically observed water molecules. (**c**) Schematic representation of catalytically important residues and their most probable interactions. (**d**) Secondary structure and sequence of minimal HHRz. (**e**) Sequence of model RNA duplex **1**. (**f**) Sequence of model RNA duplex **2**. In all panels, G12/G12-corresponding (G12*) residue, G10.1/G10.1-corresponding (G10.1*) residue and C17 residue are colored in red, magenta and green, respectively. In (**a**), (**d**–**f**), each metal ion-binding motif (A9-G10.1 motif) is surrounded by a blue box. In (**f**), the second A9-G10.1 motif in RNA duplex **2** is highlighted by a gray background. In the main text, residue numbers of HHRzs are applied to relevant residue in the model RNA duplexes with asterisk (*).

In a general sense, the cleavage reaction by HHRz proceeds as shown in Scheme 1 [23,32]. Initially, the 2′-OH at the cleavage site (the 17th residue X in HHRz, where X = C or U or A) is deprotonated (Scheme 1). Consequently, the pentacoordinated phosphorane intermediate is formed due to the nucleophilic attack of the deprotonated 2′-oxygene atom (O2′) to the neighboring phosphorus atom at the 3′ side. Finally, the leaving 5′-oxygen atom (O5′) of the 1.1th residue (N1.1) in HHRz leaves from the phosphorus atom to generate a 2′,3′-cyclic phosphate and 5′-OH at the respective cleaved ends (Scheme 1). To fully understand all of the important details of the mechanism, the catalytic role of the conserved core residues must be revealed. In particular, it is essential to determine what residues or cofactors work as acid and base to deprotonate the 2′-OH group and to protonate the leaving O5′ atom, respectively.

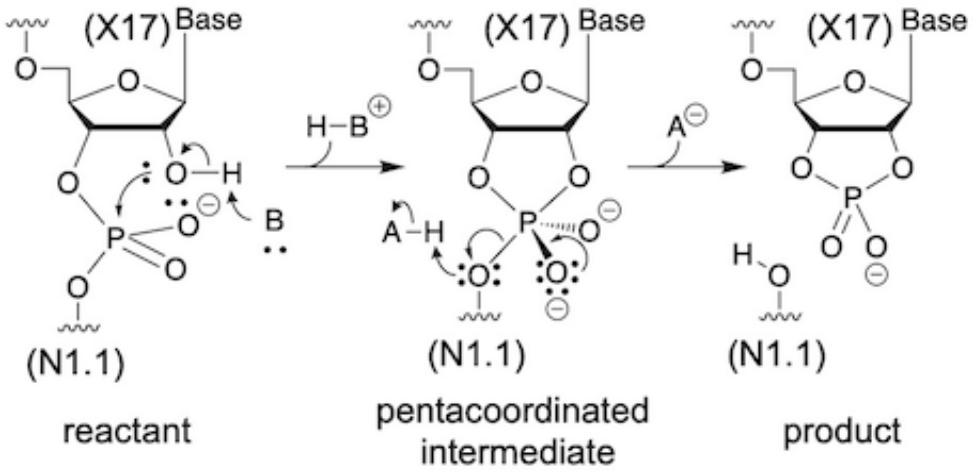

Scheme 1. Organochemical mechanism of small ribozymes.

The crystal structures of a full-length HHRz provided essential information on the function of catalytic residues [20–25]. Importantly, the nucleophile, O2′ of the X17 residue (O2′(X17)), was hydrogen bonded with the imino proton (H1) of the G12 residue (Figure 1b,c). On the basis of the crystal structures, the G12 residue is suggested to work as a base catalyst for the initial deprotonation of 2′-OH of the X17 residue (2′-OH(X17)) (the G12 base mechanism) [20–25,30–32]. However, the basicity (pK_a) of the G12 residue is currently unknown, and this property has become a missing link for the mechanistic study of HHRzs for a long time.

The assumed base catalyst of the G12 residue is included in a highly functionalized structural unit (the A9-G10.1 metal ion-binding motif), which is constituted with a sheared-type G12-A9 pair and G10.1-C11.1 pair [33–40]. Notably, our NMR studies [37–39] and a later work [40] on the A9-G10.1 motif revealed that this motif in model RNA duplexes **1** and **2** (Figure 1e,f) possessed a metal ion-binding ability independently from any other conserved residue of HHRzs. This independently expressed ability of the exclusive A9-G10.1 motif stimulates a concept that this motif itself may have a specific property, and HHRzs might simply utilize its property, employing the A9-G10.1 motif as a catalytic unit. In this case, once the pK_a value of the G12-corresponding residue (hereafter denoted as G12*) is revealed, the basicity of the base catalyst in HHRzs will be determined. Even if it is not the case, the derived pK_a value of the G12 residue will be regarded as the baselines (starting points) for a further modulation of the pK_a value in a whole HHRz system. Consequently, it is obviously important to study the intrinsic basicity (pK_a) of G12*, which is embedded in RNA duplexes **1** and **2**. In addition, the intrinsic basicity (pK_a) of G10.1* (G10.1 corresponding residue) is also an interesting topic to explore its metal ion affinity.

Furthermore, the "8–17 DNAzyme" also utilizes the sheared-type G-A pair as its catalytic unit, where its G residue works as a possible base catalyst [41,42]. Thus, it is obviously important to reveal the intrinsic basicity (pK_a) of the functionally important guanine base in the sheared-type G-A pair.

In regard to the detection of proton association/dissociation processes, those of a guanine base can be monitored spectroscopically [43–48]. The NMR chemical shift of a non-exchangeable H8 proton of purine bases is a useful probe for protonation/deprotonation processes [44]. For example, the deprotonation at N1 of guanosine residues in dinucleotides induces ~0.1 ppm upfield shift of their H8 resonances, while the protonation at N7 nitrogen induces ~1 ppm downfield shift of H8 resonances [44]. Therefore, by using H8 resonances of RNA duplexes **1** and **2**, which were already assigned [33,37–39], the pK_a values of the G12* and G10.1* residues can be analyzed.

Based on these facts, we performed pH-titration experiments of the model RNA duplexes **1** and **2** for monitoring the protonation state of the G12* and G10.1* residue

with NMR spectroscopy. From the data, in conjunction with the pre-existing kinetic and structural data, we discussed the possible relationship between catalytic activity and the derived physicochemical properties.

2. Results

2.1. pK_a Determination of G12-Corresponding Residue

To reveal the basicity of the N1 of G12* (N1(G12*)) within RNA duplex **1**, one-dimensional ^{1}H NMR spectra were recorded at various pH levels ranging from 6.60 to 10.48 (Figure 2). The resonance of H8 of G12* (H8(G12*)) was unequivocally identified owing to the assignment of all base protons and anomeric protons in the RNA duplex **1** in the previous work [33]. The H8(G12*) resonances within ^{1}H NMR spectra were labeled with an asterisk (Figure 2).

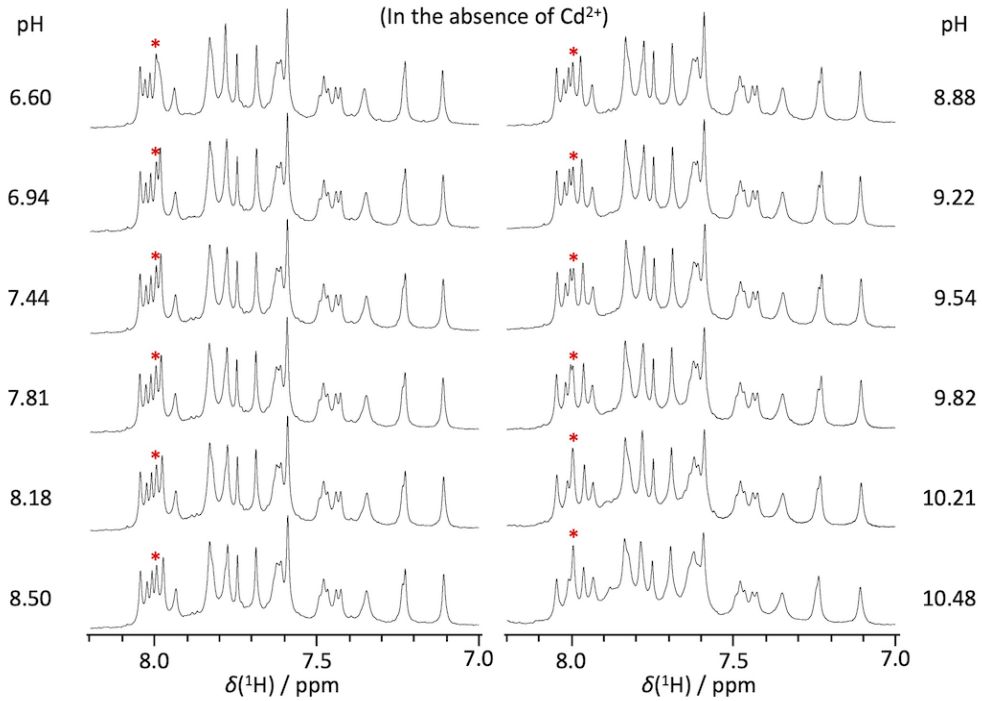

Figure 2. One-dimensional ^{1}H NMR spectra of the model RNA duplex **1** against various pH levels (basic region) in the absence of $CdCl_2$. The H8(G12*) resonance is labeled with a red asterisk in each spectrum. Although chemical shift perturbations for several resonances were observed, these resonances were assigned to terminal residues. To assure the trace of the NMR signals of base protons, ^{1}H-^{1}H NOESY and natural abundance ^{1}H-^{13}C HSQC spectra were recorded at pH 8.18 (Figures S2 and S3).

Unexpectedly, the H8(G12*) resonance was not perturbed until pH 10.48, the pH upper limit of the duplex formation (Figures 2 and 3). The deprotonation of the N1 site (N1-deprotonation) generally results in an upfield shift of the H8 resonance, as inferred from the titration data of guanosine 5′-monophosphate (5′-GMP) (Figure 3, open circles). However, the upfield shift of H8(G12*) did not occur, and deprotonation of the G12* residue was thus not evidenced. Correspondingly, the pK_a of the G12* can be confined as pK_a >> 10.48. When compared with the corresponding pK_a for 5′-GMP (pK_a (5′-GMP) 9.4) (Figure 3) [49], the basicity of the G12* residue was notably higher than that of a normal guanine base.

We further confirm whether the pK_a of N1(G12*) is affected by the presence of a divalent metal cation because the HHRz can be activated in the presence of divalent metal cation [15–17,50–54]. For this purpose, titration experiments were carried out under the Cd^{2+}-excess condition against the G10.1-A9 motif (two molar equivalents) within the pH range from 6.02 to 10.67 (Figure 4). As a divalent metal cation, Cd^{2+} was selected, since it is a strong binder for the A9-G10.1 motif with an NMR-compatible "diamag-

netic" character [37–40] and has been used for several kinetic experiments [53,55,56]. The H8(G12*) resonance was again unperturbed, except for the insignificant downfield shift above pH 9.22 (Figures 3 and 4). Since the direction of the chemical shift perturbation above pH 9.22 was opposite to that of N1-deprotonation for 5′-GMP (Figure 3, open circles) and the theoretical values (Tables S1 and S2), the observed tiny downfield shift of H8(G12*) (~0.015 ppm) was likely induced due to a transition other than the G12*-deprotonation. In fact, many resonances were perturbed above pH 9.22 (Figure 4). These perturbations are most likely attributed to Cd^{2+}-dissociation upon the metal precipitation under basic conditions judging from the similarity of the NMR spectra ($+Cd^{2+}$) at pH 10.29 (Figure 4) and the one ($-Cd^{2+}$) at pH 10.21 (Figure 2).

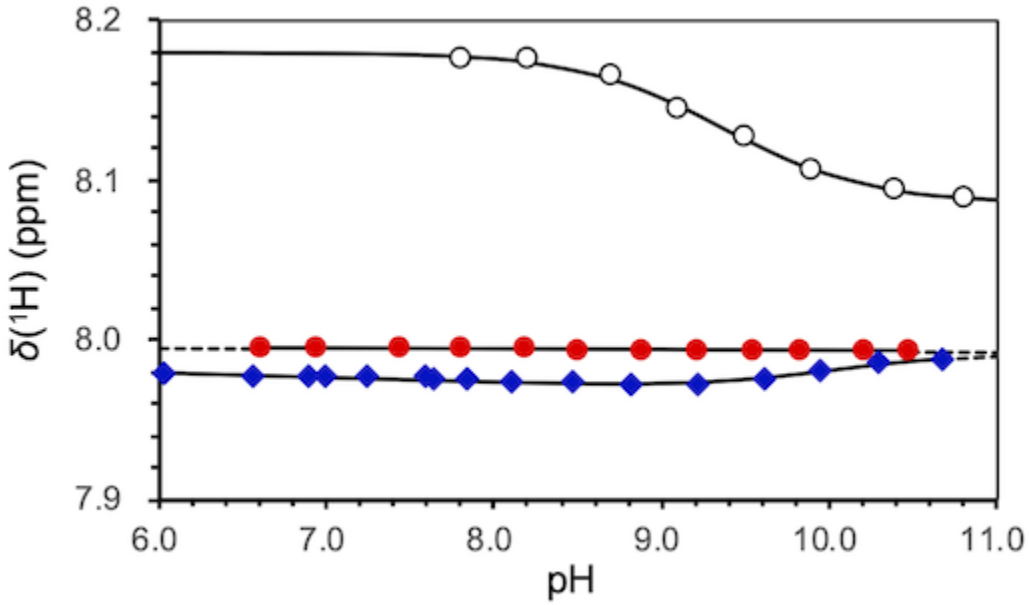

Figure 3. Plot of the chemical shift of H8(G12*) of the model RNA duplex **1** against pH (basic region). Red circle: H8(G12*) chemical shift in the absence of $CdCl_2$. Blue diamond: H8(G12*) chemical shift in the presence of $CdCl_2$. Open circle: H8(5′-GMP) chemical shift in the absence of $CdCl_2$. In the respective titration data, their corresponding theoretical curves are indicated. In the theoretical curves for model RNA duplex **1**, extrapolated theoretical curves are presented as broken lines.

To sum up the reported results so far, the unperturbed chemical shift value of H8(G12*) upon the pH changes in the absence/presence of $CdCl_2$ indicated that the basicity of G12* is considerably higher than that of a canonical guanine base such as 5′-GMP. The pK_a value of N1(G12*) should be much higher than 10.5, most likely above ~11.5 in the absence/presence of $CdCl_2$, assuming the theoretical titration curve. The current experimental data demonstrated that the N1(G12*) site is highly basic, irrespective of the presence or absence of Cd^{2+} cation. Thus, the guanine base of G12* involved in the A9-G10.1 motif was found to be intrinsically very basic. This highly basic property of G12* is notable, especially when considering that the imino proton of G12* is structurally exposed to bulk solvent due to the sheared-type G-A pairing. In general, pK_a alteration is brought by structural factors (sequestration of the protonation/deprotonation-site), or electronic effects (modulation of the electronic structure of acid/base-moiety), or by a combination of both effects. In the case of the A9-G10.1 motif, the structural factor doesn't explain the pK_a alteration as mentioned above. Here the distinguished pK_a value may be most likely attributed to the electronic effect caused by non-standard sheared-type G12-A9 base pairing and π-π stacking of the G12-A9 and G10.1-C11.1 base pairs.

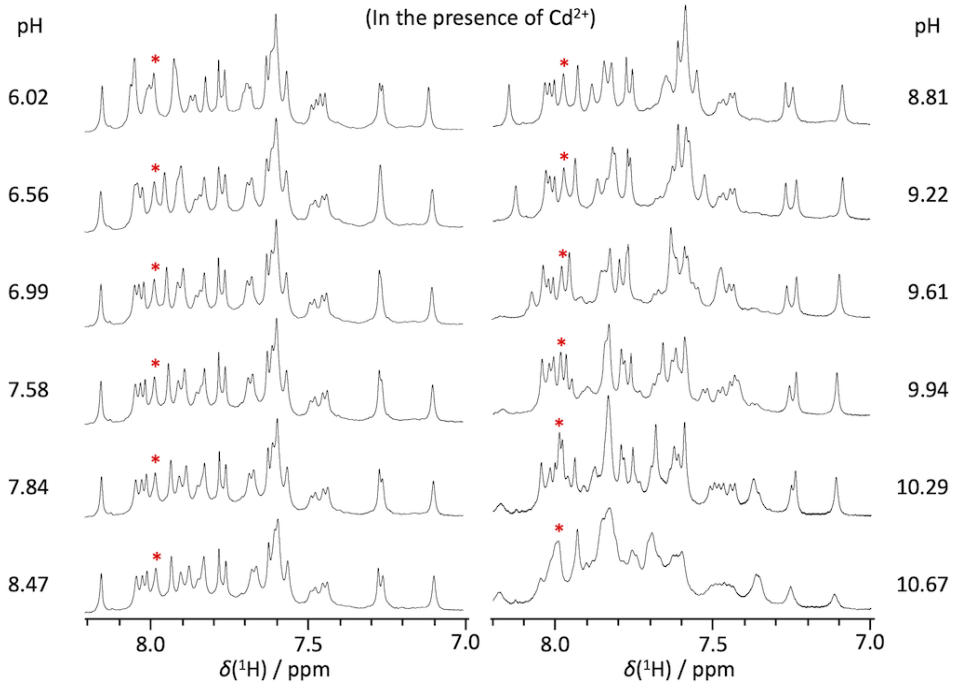

Figure 4. One-dimensional ^{1}H NMR spectra of the model RNA duplex **1** against various pH (basic region) in the presence of $CdCl_2$ (two molar equivalents (2 mM) against the metal ion-binding A9-G10.1 motif). The H8(G12*) resonance is labeled with a red asterisk in each spectrum. Although chemical shift perturbations for several resonances were observed, these resonances were assigned to terminal residues. Above pH 9.22, a metal-dissociation process due to the Cd^{2+}-precipitation under basic pH was observed.

To generalize the above observation (basicity enhancement of G12*), the basicity of G12* was studied with another similar RNA duplex (RNA duplex **2**), which also includes the A9-G10.1 motif [37–39,57]. The pH-titration experiments of RNA duplex **2** in the basic region (Figure 5) again showed negligible perturbation of the NMR chemical shift for H8(G12*), irrespective of either the presence or absence of Cd^{2+}. Thus, two independent titration experiments for RNA duplexes **1** and **2** exhibited the unperturbed chemical shift for H8(G12*) against pH, which strongly supports that no deprotonation of the N1(G12*) site occurred. To summarize, the guanine base in the A9-G10.1 motif intrinsically possesses notably basic property.

Next, theoretical calculations of the chemical shift perturbation of H8(G12*) upon the N1-deprotonation were performed in order to explore its direction and degree. For the calculations, the central four-base-pair region (two A9-G10.1 motifs) of the RNA duplex **2**, r(CGAG)$_2$, was used (Figure 1 and Figure S1). Upon N1-deprotonation, the theoretical chemical shift of H8(G12*) was shifted 0.17 ppm upfield and that of 5′-GMP was shifted 0.20 ppm upfield. These theoretical values are consistent with the experimental observation (~0.1 ppm upfield shift for H8(5′-GMP)). More importantly, the theoretical data clearly indicated that the H8(G12*) chemical shift should be notably affected upon the N1-deprotonation, and the unperturbed chemical shift of H8(G12*) during the titration experiments can be thus safely interpreted as the retention of the imino proton of G12* even at the highest pH (pH ~10.5 in the titration experiments). Considering the theoretical titration curve, the highly basic nature (pK_a > ~11.5) of the N1(G12*) site was fully supported by the theoretical calculation.

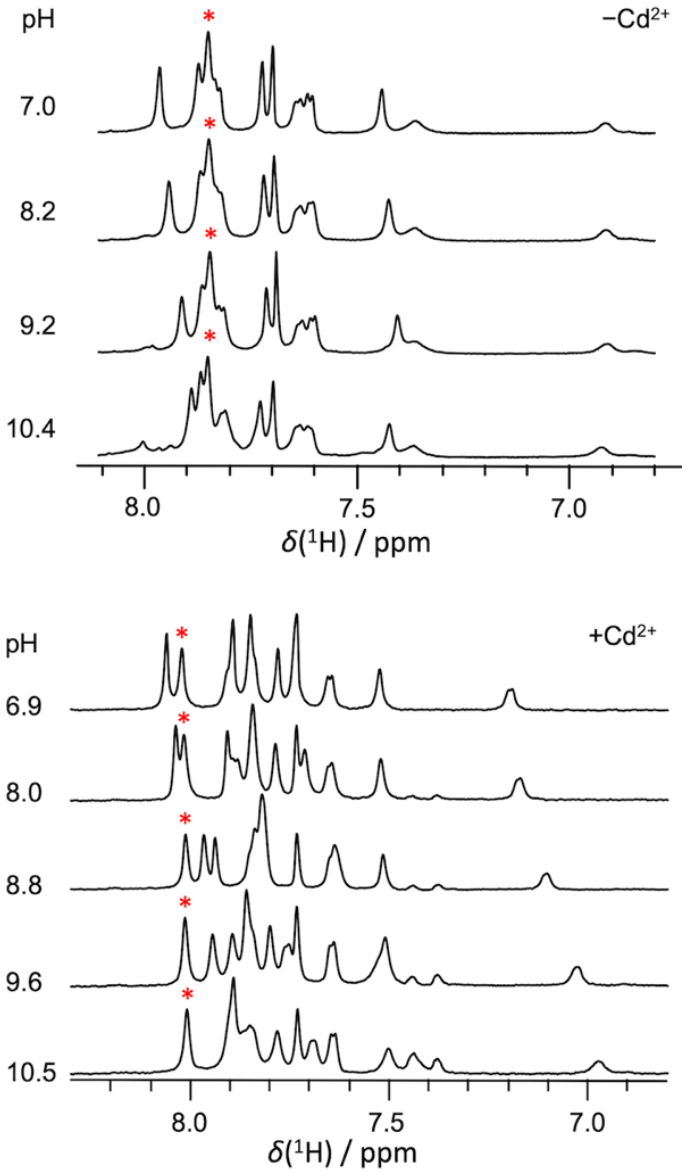

Figure 5. One-dimensional ^{1}H NMR spectra of the model RNA duplex **2** against various pH (basic region) in the absence/presence of $CdCl_2$ (two molar equivalents (2 mM) against the metal ion-binding A9-G10.1 motif). The H8(G12*) resonance is labeled with a red asterisk in each spectrum. Although chemical shift perturbations for several resonances were observed, these resonances were assigned to terminal residues. Above pH 9.22, a metal-dissociation process due to the Cd^{2+}-precipitation under basic pH was observed. The 1D ^{1}H NMR spectrum of denatured duplex **2** at pH 10.9 in the absence of $CdCl_2$ is shown in Figure S4 in the Supplementary Materials.

2.2. pK_a Determination of G10.1-Corresponding Residue

Next, we examined the basicity of the metal ion-binding site, N7 of G10.1(N7 (G10.1*)), to provide the chemical reason for the affinity of metal. The binding of N7(G10.1*) to a metal cation due to coordination-bond (Lewis acid–Lewis base interaction) is strongly correlated with the Brønsted basicity of N7(G10.1*). Therefore, the titration experiments were also performed within the acidic region. Correspondingly, the ^{1}H NMR spectra were recorded for pH that ranged from 7.36 to pH 3.57 (Figure 6). Below pH 4.25, the duplex **1** most likely underwent denaturation, which prevented the further titration experiment. Accordingly, the titration data between pH 7.36 and pH 4.40 were used for the pK_a analysis (Figure 7).

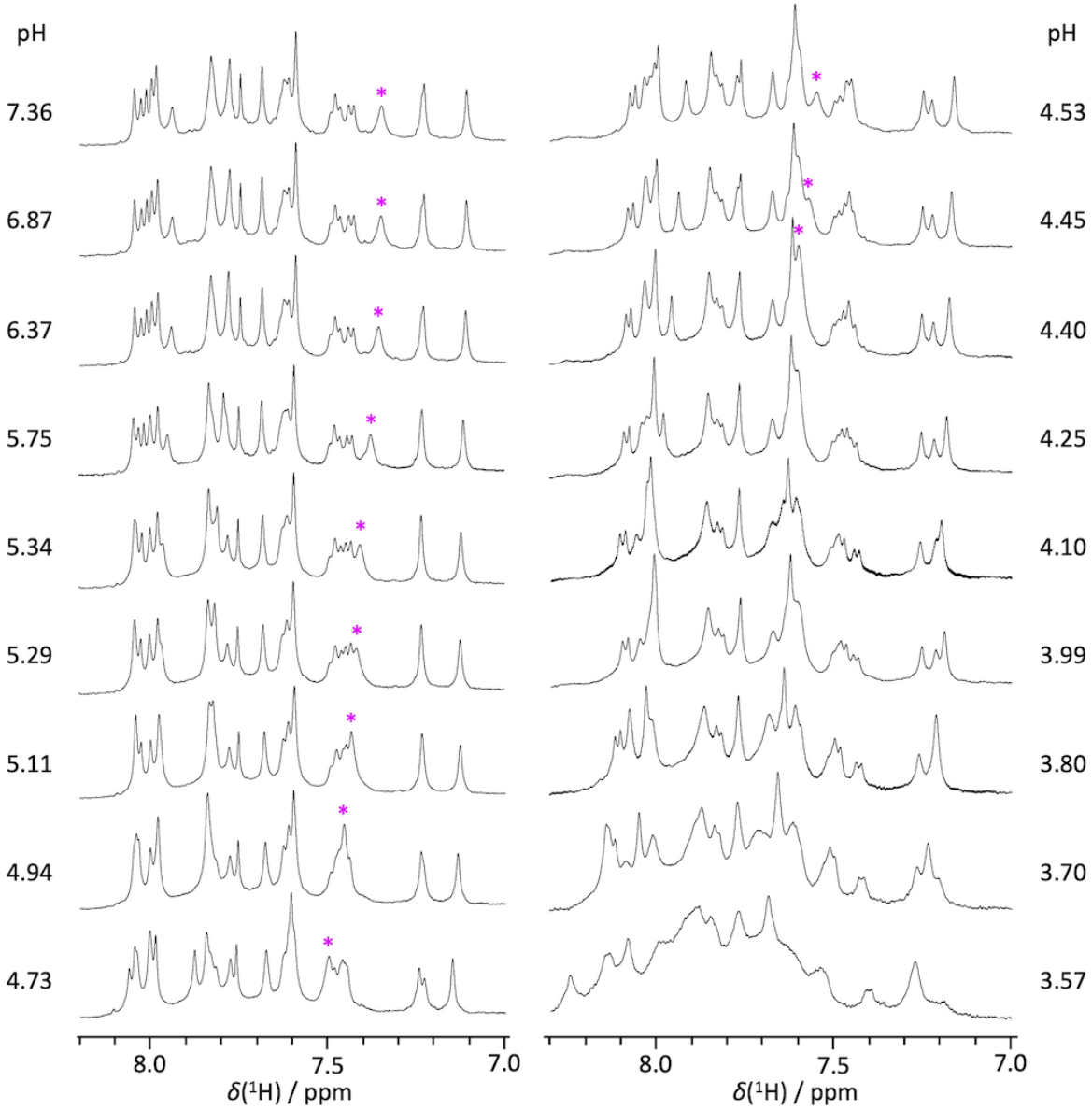

Figure 6. One-dimensional ^{1}H NMR spectra of the model RNA duplex **1** against various pH (acidic region) in the absence of $CdCl_2$. The H8(G10.1*) resonance is labeled with a magenta asterisk in each spectrum. Although chemical shift perturbations for several resonances except for H8(G10.1*) resonance were observed, these resonances were assigned to terminal residues. Below pH 3.70, denaturation of the duplex was evident. To assure the trace of the NMR signals of base protons, a natural abundance ^{1}H-^{13}C HSQC spectrum was recorded at pH 4.40 (Figure S5).

The best-fit theoretical curve indicated that the pK_a value for N7(G10.1*) was 4.4 (Figure 7). This value was higher than pK_a 2.4 for a normal guanine base [49] by approximately two pK_a units. Accordingly, the N7(G10.1*) metal ion-coordination site is more basic than a normal guanine base. This enhanced Brønsted basicity should increase the Lewis basicity of N7(G10.1*), which likely explains its strong metal affinity. The existence of another metal ligand of the phosphate group of the A9-corresponding residue (PO_4(A9*)) further makes the A9-G10.1 motif a well-organized metal ion-binding motif due to the chelation effect. In total, the enhanced basicity of N7(G10.1*) and the existence of the phosphate group of the A9 residue as the second ligand are the chemical reasons for the extraordinary metal affinity of the A9-G10.1 motif.

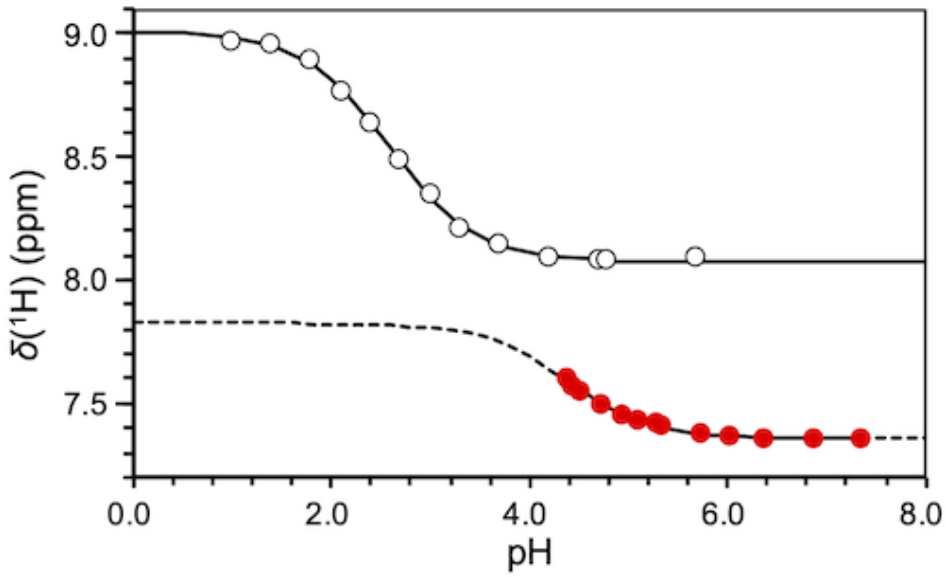

Figure 7. Plot of the chemical shift of H8(G10.1*) of the model RNA duplex **1** against pH (acidic region) in the absence of $CdCl_2$. Red circle: H8(G10.1*) chemical shift. Open circle: H8(5′-GMP) chemical shift. In the respective titration data, their corresponding theoretical curves are indicated. In the theoretical curves for model RNA duplex **1**, extrapolated theoretical curves are presented as broken lines.

In total, we have characterized the basicity of two functionally important guanosine residues, G12* and G10.1*, and demonstrated the extraordinarily basicity of N1(G12*) and N7(G10.1). It means that we obtain the intrinsic basicity of these sites in an isolated functional unit extracted from HHRzs.

3. Discussion

3.1. Experimental pK_a Values of Functionally Important Residues

We have explored the pK_a values of two functionally important guanosine residues, G12* and G10.1*, in the catalytic unit of HHRzs to characterize their intrinsic physicochemical properties in relation to the catalytic mechanism of HHRzs. From the results, N7(G10.1*) was found to exhibit pK_a 4.4, which is approximately two pK_a units higher than a normal guanine base. This enhanced Brønsted basicity is likely one of the reasons for the high metal affinity of N7(G10.1*) (=increased Lewis basicity). Next, in regard to the basicity of the catalytic site, N1(G12*) was found to be pK_a >> 10.48. Assuming the theoretical titration curve, its pK_a value would be higher than 11.5, which is two pK_a units higher than a normal guanine base. We would like to emphasize that pK_a 11.5 is the minimum value, and its actual value could be higher. It is noteworthy that the mutual correlation between the chemical shifts of H8(G12*) and H8(G10.1*) was not observed. This implies that the direct interaction of G12* and G10.1* residues is very weak and the altered pK_a values of N1(G12*) and N7(G10.1*) are most likely due to some effect(s) other than the direct interaction of the two residues. As a remark, current analyses rely on the ^{1}H NMR chemical shift perturbations, which may, in principle, be affected by various structural effects. For more solid pK_a analysis, an ^{15}N NMR study would be desirable in the future, although there is no obvious inconsistency between the experimental data and the current interpretation.

Based on the derived data from the RNA duplexes **1** and **2**, the intrinsic pK_a values of G10.1* and the minimal pK_a value of G12* were obtained for the exclusive catalytic unit itself. The pK_a values of the functionally important guanosine residues, G12* and G10.1*, deviated significantly from the standard values. Such modulations are often observed in catalytic residues of enzymes, and in general, the modulated properties are

efficiently used in their catalysis [48]. Therefore, the derived property of G12* and G10.1* in RNA duplexes **1** and **2** might be an intrinsic nature of the catalytic unit, although their pK_a values within the full-length HHRz could be further modulated owing to additional interactions in the whole HHRz system. Even in this case, the derived physicochemical values can be regarded as the baselines (starting points) for the further modulations in the whole HHRz system.

3.2. Ground State Structure Inferred from the Crystal Structure

Next, we would like to discuss the relationship between the catalytic mechanism and the newly determined physicochemical property of G12* on the basis of the three-dimensional (3D) structure of the full-length HHRz. When several possible mechanisms are considered, a common ground state should be defined. Otherwise, their comparison becomes impossible due to the lack of an energetic reference.

In the 3D structure of full-length HHRz [20–25], the hydrogen-bond network around the cleavage site can be drawn as shown in Figure 1c. The relevant ground state (before the catalysis) was drawn accordingly (Scheme 2), assuming normal pK_a values for the imino proton of guanine and the 2′-hydroxy group of ribose [43,49]. In the assumed ground state, the imino proton of the G12 residue (H1(G12)) is bound for N1 of G12 (N1(G12)), and hydrogen-bonded with O2′(X17). As a result, the hydroxy proton, H2′(X17), may point to the non-bridging oxygen atoms (*pro-*R_P/*pro-*S_P oxygen atoms) of the scissile phosphate group. In fact, O2′(X17) was found within a possible hydrogen-bonding distance with the *pro-*R_P/*pro-*S_P oxygen atoms in crystal [20]. Thus, the structure of the assumed ground state looks reasonable, and the energetic standard with the relative potential energy for comparing the respective possible mechanisms was obtained.

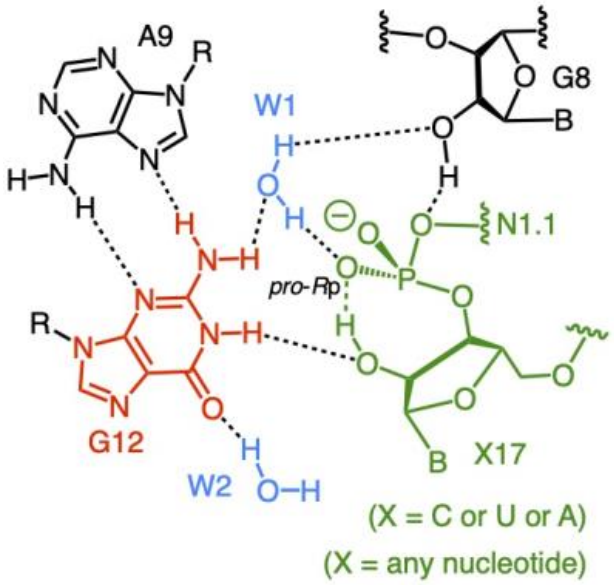

Scheme 2. Ground state of HHRzs before the catalysis. The cleavage site (X17) and the nucleophile activator (G12) are colored in green and red, respectively.

3.3. Two Major Possible Mechanisms

Historically, two kinds of mechanisms were proposed (Figure 8). One is the mechanism where the G12 residue works as a base for proton abstraction from 2′-OH(X17) (G12 base mechanism, Figure 8a) [20–25,30–32]. The other is the so-called triester-like mechanism (Figure 8b) [58–60].

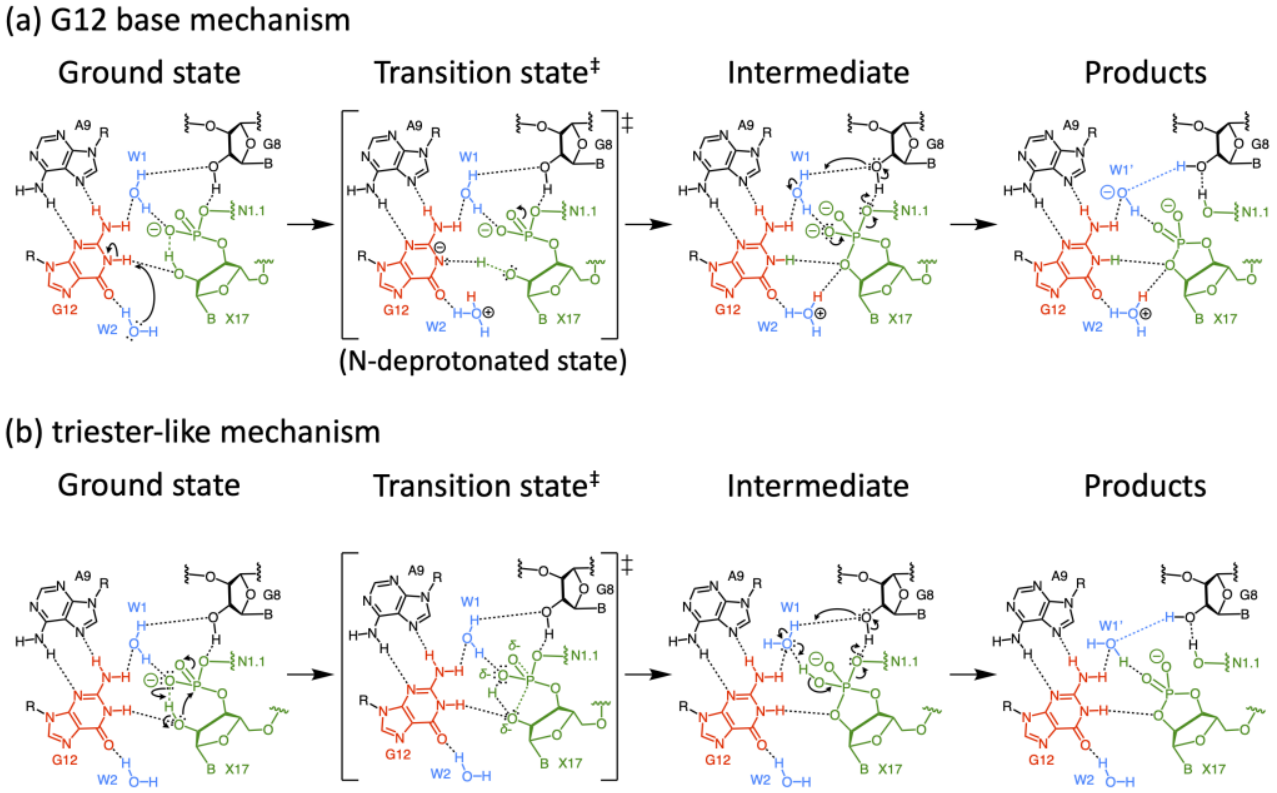

Figure 8. Schematic representation of possible reaction pathways based on the crystal structure (PDB ID: 2OEU [21]). (**a**) Possible reaction pathway of the G12 base mechanism. (**b**) Possible reaction pathway of the triester-like mechanism. In all panels, the positions of hydrogen atoms are estimated from the crystal structure, assuming typical pK_a values for the respective sites [43,44,49]. Crystallographically observed water molecules, which may participate in the catalysis, are drawn. Even after the proton transfer, the colors of protons are retained in their original residue's/molecule's colors.

In the G12 base mechanism, the imino proton of G12 is deprotonated, and the subsequent proton abstraction from 2′-OH(X17) with the nucleophilic attack of O2′(X17) occurs to give the pentacoordinated phosphorane intermediate. The leaving group of O5′ of N1.1 (O5′(N1.1)) is dissociated from the intermediate with the aid of a proton donation from the 2′-OH group of G8 (2′-OH(G8)). As a result, the substrate RNA strand is cleaved.

In the case of the triester-like mechanism, H2′ of X17 (H2′(X17)) moves to a non-bridging oxygen of the scissile phosphate with simultaneous nucleophilic attack of O2′(X17) to the phosphorus atom to give the pentacoordinated phosphorane intermediate. Subsequent reactions are similar to the G12 base mechanism.

3.4. Correlation of Possible Reaction Mechanisms with Kinetic Data

From the kinetic studies, pH-dependent catalysis was reported, in which the catalytic activity of HHRzs was enhanced with the increase of pH [16,27,31]. It is interpreted that the pH increase brings the increase in the concentration of the deprotonated base (active form of the base catalyst), which results in the reaction rate enhancement. Therefore, when the crystal structure revealed the existence of the hydrogen bond between H1(G12) and O2′(X17) (Figure 1b,c), the G12 residue was postulated as the base catalyst (the G12 base mechanism) [16,20–25,31]. The existence of the base catalyst in the G12 base mechanism is consistent with the existing kinetic data. On the other hand, the triester-like mechanism does not include an explicit base catalyst, which may contradict the kinetic observation. However, even without a base catalyst, the pH dependence can be explained as follows. Firstly, protons can work as a mask for the non-bridging oxygens of the scissile phosphate as a reaction blocker. Upon the pH increase, the concentration of protons in a bulk is lowered,

and this decrease in the concentration of the reaction blocker may facilitate the proton transfer of H2′(X17) to the phosphate oxygen. In addition, a possible base catalyst was found for the triester-like mechanism (see Section 3.6 for details). Thus, the pH-dependent reaction rate enhancement can be explained, even in the triester-like mechanism.

In reference [32], an observable rate constant, kobs, is thought to be proportional to both the fraction of the deprotonated base (active form of base catalyst) and the acid catalyst (the proton donor to the leaving oxygen atom).

$$k_{obs} = k_{cat} \bullet f_B \bullet f_A \quad (1)$$

where k_{cat}, f_B and f_A represent an intrinsic rate constant, a fraction of a deprotonated base ($0 < f_B < 1$) and a fraction of a protonated acid ($0 < f_A < 1$).

For $f_B = 1$ and $f_A = 1$, the maximum activity is observed, and Equation (1) becomes $k_{obs} = k_{cat}$. In the case of HHRzs, the acid catalyst is thought to be the 2′-OH (G8). Therefore, under the experimentally examined pH range, the fraction of a protonated acid (f_A) can be assumed $f_A \approx 1$, and Equation (1) becomes

$$k_{obs} \approx k_{cat} \bullet f_B \quad (1a)$$

Based on Equation (1a), we would like to investigate the two possible mechanisms. As for the G12 base mechanism, a fraction of the N1-deprotonated G12 base (f_B) is increased upon the pH increase, and it is consistent with the observed rate enhancement. However, caution must be taken for the absolute value of f_B. If we assume that the pK_a value of the G12 residue in full-length HHRzs is the same as or higher than that of G12* in the model system, a fraction of the deprotonated G12 base could be significantly lowered, which may result in a decrease in the observed rate constant k_{obs}. To maintain a reasonable k_{obs} value, the intrinsic rate constant k_{cat} should be enlarged.

From the energetic point of view, the energetic increase due to the N1-deprotonation, E_{dep}, can be formulated as follows:

$$E_{dep} = -RTlnK_a \quad (2)$$

Assuming pK_a = 11.5 for N1(G12) in a full-length HHRz and the temperature = 298 K, E_{dep} becomes 65.6 kJ•mol^{-1} (15.7 kcal•mol^{-1}). Thus, the possible high pK_a value of N1(G12) may bring large E_{dep} and a significant increase in the activation energy of the first transition state (TS1), as shown in Figure 9, which may not be feasible for the cleavage reaction. However, in this case, the possible large k_{cat} value in Equation (1a) due to the highly basic nature of the G12 base may compensate for this situation. Thus, the accurate estimation of the final observable rate constant, k_{obs} (k_{cat}•f_B product), is not easy.

Next, in the triester-like mechanism, such a deprotonation process is not included. During the course of the triester-like mechanism, the G12 residue does not experience deprotonation. Instead, H1(G12) is hydrogen-bonded with O2′(X17), whose negative charge is transiently accumulated in TS1. As a result, the potential energy of the TS1 may be lowered, and this would be the catalytic role of G12 in the triester-like mechanism. A similar electrostatic stabilization mechanism was proposed for the hairpin ribozyme from several experimental results [47,61]. There might be a possibility that a common cleavage strategy might be utilized by small ribozymes.

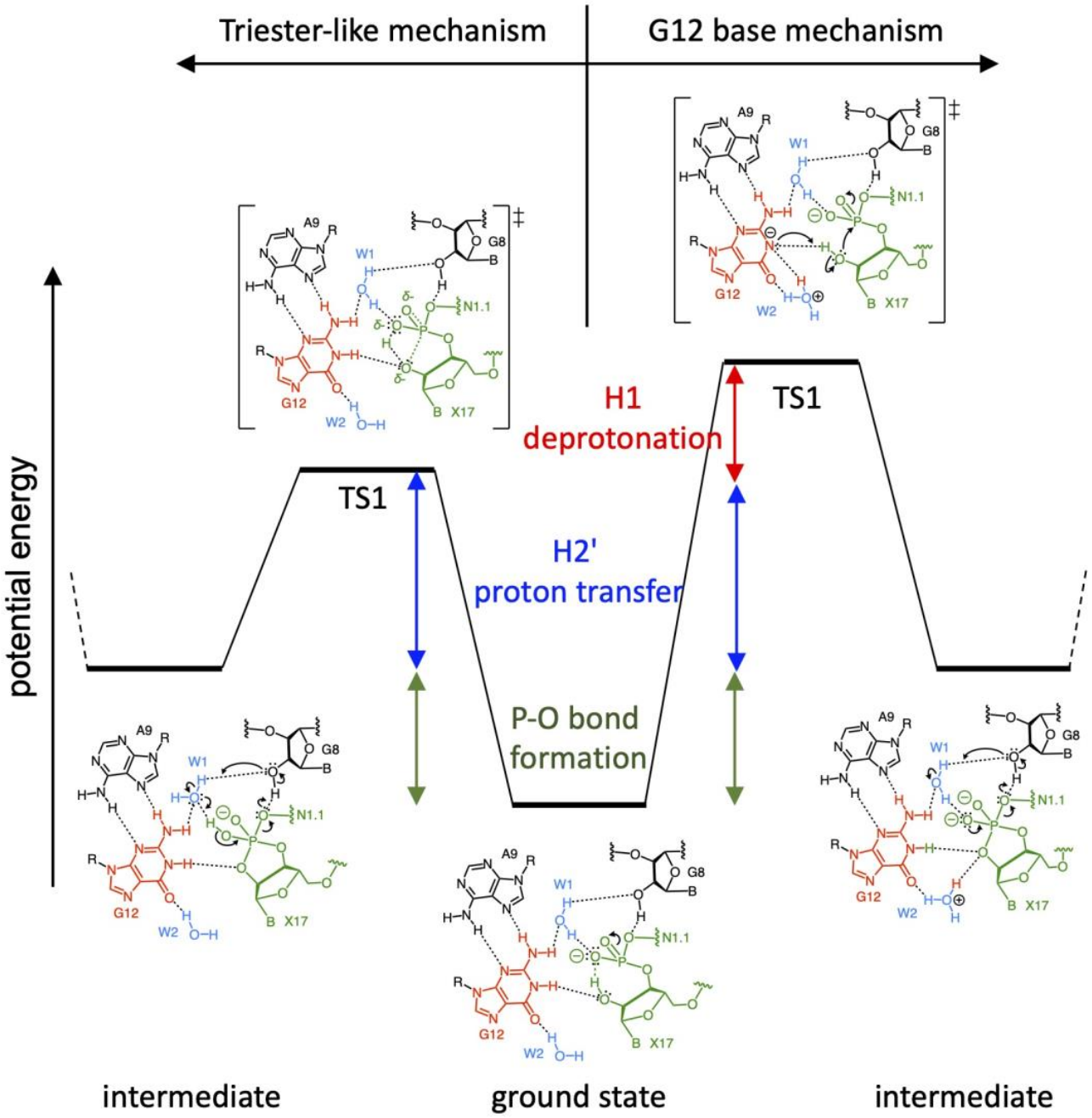

Figure 9. Potential energy profiles of the G12 base mechanism and triester-like mechanism. Energetic contributors for the first transition state are indicated with arrows.

3.5. Correlation of Possible Reaction Mechanisms with Thio-Effect

Before entering thio-effect, the related structural features must be described. On the basis of the crystal structure [21], a water molecule (W1) bridged the *pro-R*$_P$ oxygen atom and 2′-OH(G8) (Figure 1b,c and Scheme 2). This 2′-OH(G8) is also known to work as "an acid catalyst", which facilitates the proton transfer from 2′-OH(G8) to the leaving O5′(N1.1) [32]. Therefore, in the triester-like mechanism, once the *pro-R*p oxygen atom captures the 2′-hydroxy proton, H2′(X17), the captured proton would be efficiently transferred to the final destination of O5′(N1.1) via W1 through the hydrogen bond network (Figure 8b).

With regard to the thio-effect, the thio-substitution of the *pro-R*p oxygen of the scissile phosphate group diminished the reaction rate of HHRzs [55,56,62]. Based on this observation, when the *pro-R*$_P$ oxygen atom is thio-substituted, the proton transfer step from

O2′(X17) to the sulfur atom and/or that from the sulfur atom to W1 could be inhibited due to a steric effect or basicity change of the *pro-R*$_P$ atom, as was pointed out in the literature [58]. Next, the thio-substitution of the *pro-S*$_p$ oxygen did not affect the cleavage rate as much [55,56,62]. This observation is also consistent with the triester-like mechanism, since the *pro-S*$_p$ position does not participate in the hydrogen bond network between the *pro-R*$_P$ oxygen atom and O5′(N1.1). Thus, the triester-like mechanism can reasonably explain the thio-effect. In the case of the G12 base mechanism, by the oxygen–sulfur substitution at the *pro-R*p site, the acidity of W1 may be affected through the sulfur–W1 hydrogen bond. It may eventually affect the proton relay from 2′-OH(G8) to leaving O5′(N1.1). In this way, the relationship between the G12 base mechanism and thio-effect also can be rationalized. Thus, the thio-effect does not become solid evidence to exclude one of the mechanisms.

3.6. Correlation of Possible Reaction Mechanisms with Their Intermediate and Product States

Firstly, the intermediate state of the respective mechanisms is considered. In the G12 base mechanism, the chemical structure of its pentacoordinated phosphorane intermediate is a dianionic form. This structure elevates its potential energy inferred from the pK_a[1] (6.5–11.0) and pK_a[2] (11.3–15.0) of the pentacoordinated phosphorane intermediate [63]. On the contrary, the chemical structure of the pentacoordinated phosphorane intermediate for the triester-like mechanism is a monoanionic form due to the proton transfer from 2′-OH(X17). This protonation of the intermediate brings stabilization of the intermediate. Though this stabilization of the intermediate may not necessarily be related to the reaction rate, this intermediate stability of the triester-like mechanism could lower the activation energies before and after the intermediate state. In addition, because the pentacoordinated phosphorane intermediate possesses more basic property (higher pK_a values) than a normal phosphodiester group [63], it can be regarded that the phosphate group at TS1 on the way to the pentacoordinated phosphorane works as "the base catalyst". Such a hidden base thus exists even in the case of the triester-like mechanism.

Secondly, the product state of the respective mechanisms is considered. In the G12 base mechanism, chemical structures of W1 and W2 become a hydroxide anion and an oxonium cation, respectively (Figure 8a). This ionic charge-separated state would increase the potential energy of the product. On the other hand, in the triester-like mechanism, the chemical structures of W1 and W2 in their product state retain their initial state (Figure 8b), and no energetic increase due to W1 and W2 is expected.

3.7. Possible Reaction Mechanisms

Based on the discussion in this study, both the G12 base mechanism and the triester-like mechanism were found to be rationalized against the currently available experimental data. As an interesting remark, a reasonable energetic profile of the catalytic reaction of the hairpin ribozyme was also shown for the triester-like mechanism from the theoretical calculation [64]. Accordingly, in addition to the currently assumed G12 base mechanism, the triester-like mechanism should also be regarded as a possible candidate of the mechanism of HHRzs.

3.8. Conclusions

The current spectroscopic study revealed the intrinsic pK_a values of functionally important sites of the G12/G10.1-corresponding residues in the catalytic unit of HHRzs. The G10.1-corresponding residue showed a notably basic character compared to a guanosine monomer by ~2 pK_a unit, which is responsible for high metal affinity (=Lewis basicity). More interestingly, the pK_a value of the G12-corresponding residue is extraordinarily basic, and a fraction of the deprotonated G12 residue can be calculated under an arbitrary pH, which could be a benchmark for evaluating the reaction mechanisms of HHRzs in the future. Thus, thermodynamic/equilibrium analyses and careful reconsiderations of existing experimental data illuminated that the triester-like mechanism is also a possible one, besides the currently assumed G12 base mechanism. Through the consideration in

this study, it is reasonably concluded that a thermodynamic/equilibrium approach would provide an independent measure that can be an outstanding pivot point to evaluate the possible mechanisms of HHRzs.

4. Materials and Methods

4.1. Preparations of RNA Oligomers and NMR Measurements

The RNA oligomers used in this study were synthesized and purified as described in the literature [33,65].

The solution for the titration experiments of RNA duplex **1** contained 1 mM RNA duplex **1**, and 100 mM NaCl in D_2O. In the titrations under basic conditions without $CdCl_2$, 2 mM Na-phosphate pH 6.94 was initially added, and further basic pH conditions were adjusted by the direct titrations with NaOD in D_2O. In the titrations under basic conditions with 2 mM $CdCl_2$, no buffer was added so as not to precipitate Cd^{2+} cation, and further basic pH conditions were adjusted by the direct titrations with NaOD in D_2O. In the titrations under acidic conditions without $CdCl_2$, the pH conditions were adjusted by the direct titrations with D_2SO_4 in D_2O. The 1D ^1H NMR spectra at the respective pH values were recorded on a Bruker Advance III HD 500 MHz spectrometer equipped with a BBO cryogenic probe at 303 K (Bruker, Billerica, MA, USA). Each spectrum was recorded with 327,68 complex points for a spectral width of 16,025.641 Hz.

The solutions for the titration experiments of RNA duplex **2** contained (solution 1) 1.0 mM RNA duplex **2**, 50 mM NaCl in D_2O and (solution 2) 0.25 mM RNA duplex **2**, 50 mM NaCl, 1.0 mM $Cd(NO_3)_2$ in D_2O. In both solutions, no buffer was added in the titration experiments, and the pH conditions were adjusted by the direct titrations with D_2SO_4 in D_2O for acidic conditions and NaOD in D_2O for basic conditions, respectively. The 1D ^1H NMR spectra at the respective pH values were recorded on a JEOL ECA600 spectrometer at 298 K (JEOL, Japan). Each spectrum was recorded with 8192 real points for a spectral width of 6600 Hz.

4.2. Equilibrium Analyses for Titration Data

In the case of titration experiments, experimentally observed chemical shifts, δ_{obs}, follows the theoretical Equation (3) shown below.

$$\delta_{obs} = (\delta_{protonated} + \delta_{deprotonated} \bullet 10^{(pH-pKa)})/(1 + 10^{(pH-pKa)}) \quad (3)$$

where $\delta_{protonated}$, $\delta_{deprotonated}$ and pK_a denote the theoretical limiting value of the chemical shift for the protonated state, the theoretical limiting value of the chemical shift for the deprotonated state and the pK_a value for the corresponding reaction. The respective titration data were fitted to Equation (3), using $\delta_{protonated}$, $\delta_{deprotonated}$ and pK_a as variable parameters for the least square fitting. All calculations were performed using Microsoft Excel for Mac version 16.44.

4.3. Theoretical Calculations of NMR Chemical Perturbations

The model RNA molecule for the chemical shift calculations was derived using the structure of RNA duplex with PDB ID 1YFV [66] that involved the same as the central four base pairs of RNA duplex **2**. The four-base-paired RNA fragment $r(CGAG)_2$ from the 1YFV including two Watson–Crick G-C and two sheared-type G-A pairs was geometry optimized with the QM/MM (B3LYP/6-31G++**:OPLS2005) method as implemented in the Jaguar 8.2, Impact 6.1 and Qsite 6.1 computational programs (Figure S1) [67–74]. The energy-minima structures were confirmed with the vibrational frequency calculations. The NMR chemical shift of the H8 of the guanine base in the G-A pair was calculated for the paired G-A nucleotides that were derived from the QM part within the geometry optimized $r(CGAG)_2$ model (Figure S1). The model of the 5′-GMP derived from the G-A pair involving both the neutral and the N1-deprotinated guanine base (G) was geometry optimized with the B3LYP method, 6-311+g(d,p) basis [75] and the SMD implicit water solvent [76]. The calculations of NMR chemical shielding of the H8 atom of G, σ(H8), both in the G-A pair

and in 5′-GMP, employed the GIAO approach [77], B3LYP method, 6-311+g(d,p) basis and the SMD implicit water solvent. The NMR chemical shift change of H8 in G, $\Delta\delta$(H8), due to the N1-deprotoantion of G, was calculated assuming the same NMR reference for the two states of G in accordance with the experiment as follows (Tables S1 and S2):

$$\Delta\delta\ (\text{H8}) = \delta\ (\text{H8 in N1-deprotonated G}) - \delta\ (\text{H8 in neutral G}) \quad (4)$$

$$= \sigma(\text{H8 in neutral G}) - \sigma(\text{H8 in N1-deprotonated G}). \quad (5)$$

Supplementary Materials: The following are available online at https://www.mdpi.com/article/10.3390/biophysica2030022/s1, Figure S1: The four-base-paired RNA duplex derived from the 1YFV RNA duplex, Figure S2: The ^{1}H-^{1}H NOESY spectrum of the RNA duplex 1 at pH 8.18 in the absence of $CdCl_2$. Figure S3: The natural abundance ^{1}H-^{13}C HSQC of the RNA duplex 1 at pH 8.18 in the absence of $CdCl_2$. Figure S4: The 1D ^{1}H NMR spectra of duplex 2 under pH 10.9, 10.4 and 10.9. Figure S5: The natural abundance ^{1}H-^{13}C HSQC of the RNA duplex 1 at pH 4.4. Table S1: Chemical shielding calculated for H8 atom in G in ppm, Table S2: Chemical shielding calculated for H8 atom in G in ppm.

Author Contributions: Conceptualization, Y.T.; data curation, Y.T., V.S., T.S.K., C.K. and Y.H.; formal analysis, Y.T., M.M. and Y.H.; funding acquisition, Y.T. and V.S.; investigation, Y.T., T.S.K., V.S., C.K. and Y.H.; methodology, Y.T., D.Y., S.M., T.Y., T.S.K., V.S., C.K. and Y.H.; project administration, Y.T.; supervision, Y.T.; validation, Y.T. and C.K.; writing—original draft, Y.T.; writing—review and editing, Y.T., M.M., T.S.K., V.S. and C.K. All authors have read and agreed to the published version of the manuscript.

Funding: This research was supported by Human Frontier Science Program (Young Investigator Grant to Y.T and V.S.) from the Human Frontier Science Program Organization, France; grant-in-aid for Scientific Research (C) (22K05320, 19K05705 and 20550145 to Y.T.) and (B) (24310163 to Y.T.) from MEXT, Japan.

Informed Consent Statement: Not applicable.

Data Availability Statement: Not applicable.

Acknowledgments: The authors would like to extend their appreciation to Katsuyuki Nakashima and Yasuko Okamoto (Center for Instrumental Analysis) for their instrumental support (Bruker Advance III HD 500 MHz NMR spectrometer).

Conflicts of Interest: The authors declare no conflict of interest.

References

1. Cech, T.R.; Zhang, A.J.; Grabowski, P.J. In vitro splicing of the ribosomal RNA precursor of Tetrahymena: Involvement of a guanosine nucleotide in the excision of the intervening sequence. *Cell* **1981**, *27*, 487–496. [CrossRef]
2. Guerrier-Takada, C.; Gardiner, K.; Marsh, T.; Pace, N.; Altman, S. The RNA moiety of ribonuclease P is the catalytic subunit of the enzyme. *Cell* **1983**, *35*, 849–857. [CrossRef]
3. Prody, G.A.; Bakos, J.T.; Buzayan, J.M.; Schneider, I.R.; Bruening, G. Autolytic processing of dimeric plant virus satellite RNA. *Science* **1986**, *231*, 1577–1580. [CrossRef] [PubMed]
4. Hutchins, C.J.; Rathjen, P.D.; Forster, A.C.; Symons, R.H. Self-cleavage of plus and minus RNA transcripts of Avocado sunblotch viroid. *Nucleic Acids Res.* **1986**, *14*, 3627–3640. [CrossRef]
5. Epstein, L.M.; Gall, J.G. Self-cleaving transcripts of satellite DNA from the newt. *Cell* **1987**, *48*, 535–543. [CrossRef]
6. Forster, A.C.; Symons, R.H. Self-cleavage of plus and minus RNAs of a virusoid and a structural model for the activate site. *Cell* **1987**, *49*, 211–220. [CrossRef]
7. Uhlenbeck, O.C. A small catalytic oligonucleotide. *Nature* **1987**, *328*, 596–600. [CrossRef]
8. Hertel, K.J.; Pardi, A.; Uhlenbeck, O.C.; Koizumi, M.; Ohtsuka, E.; Uesugi, S.; Cedergren, R.; Eckstein, F.; Gerlach, W.L.; Hodgson, R.; et al. Numbering system for the hammerhead. *Nucleic Acids Res.* **1992**, *20*, 3252. [CrossRef]
9. PabonPena, L.M.; Yi, Z.; Epstein, L.M. Newt satellite-2 transcripts self-cleavage by using an extended hammerhead structure. *Mol. Cell. Biol.* **1991**, *11*, 6109–6115.
10. Garrett, T.A.; PabonPena, L.M.; Gokaldas, N.; Epstein, L.M. Novel requirements in peripheral structures of the extended satellite 2 hammerhead. *RNA* **1996**, *2*, 699–706.

11. Zhang, Y.; Epstein, L.M. Cloning and characterization of extended hammerheads from a diverse set of caudate amphibians. *Gene* **1996**, *172*, 183–190. [CrossRef]
12. Jimenez, R.M.; Delwart, E.; Lupták, A. Structure-based Search Reveals Hammerhead Ribozymes in the Human Microbiome. *J. Biol. Chem.* **2011**, *286*, 7737–7743. [CrossRef]
13. Perreault, J.; Weinberg, Z.; Roth, A.; Popescu, O.; Chartrand, P.; Ferbeyre, G.; Breaker, R.R. Identification of Hammerhead Ribozymes in All Domains of Life Reveals Novel Structural Variations. *PLoS Comput. Biol.* **2011**, *7*, 13. [CrossRef]
14. Hammann, C.; Lupták, A.; Perreault, J.; de la Pena, M. The ubiquitous hammerhead ribozyme. *RNA* **2012**, *18*, 871–885. [CrossRef]
15. Khvorova, A.; Lescoute, A.; Westhof, E.; Jayasena, S.D. Sequence elements outside the hammerhead ribozyme catalytic core enable intracellular activity. *Nat. Struct. Biol.* **2003**, *10*, 708–712. [CrossRef]
16. Canny, M.D.; Jucker, F.M.; Kellogg, E.; Khvorova, A.; Jayasena, S.D.; Pardi, A. Fast cleavage kinetics of a natural hammerhead ribozyme. *J. Am. Chem. Soc.* **2004**, *126*, 10848–10849. [CrossRef]
17. Osborne, E.M.; Schaak, J.E.; DeRose, V.J. Characterization of a native hammerhead ribozyme derived from schistosomes. *RNA* **2005**, *11*, 187–196. [CrossRef]
18. Kuriyama, M.; Kondo, Y.; Tanaka, Y. Pseudoknot interaction-mediated activation of type I hammerhead ribozyme: A new class of gene-therapeutic agents. *Nucleosides Nucleotides Nucleic Acids* **2019**, *33*, 466–480. [CrossRef]
19. Yamada, M.; Tanaka, Y. Structure-activity relationship of pseudoknot-type hammerhead ribozyme reveals key structural elements for enhanced catalytic activity. *Nucleosides Nucleotides Nucleic Acids* **2020**, *39*, 245–257. [CrossRef]
20. Martick, M.; Scott, W.G. Tertiary contacts distant from the active site prime a ribozyme for catalysis. *Cell* **2006**, *126*, 309–320. [CrossRef]
21. Martick, M.; Lee, T.S.; York, D.M.; Scott, W.G. Solvent structure and hammerhead ribozyme catalysis. *Chem. Biol.* **2008**, *15*, 332–342. [CrossRef]
22. Chi, Y.I.; Martick, M.; Lares, M.; Kim, R.; Scott, W.G.; Kim, S.H. Capturing hammerhead ribozyme structures in action by modulating general base catalysis. *PLoS Biol.* **2008**, *6*, e234. [CrossRef]
23. Anderson, M.; Schultz, E.P.; Martick, M.; Scott, W.G. Active-site monovalent cations revealed in a 1.55-A-resolution hammerhead ribozyme structure. *J. Mol. Biol.* **2013**, *425*, 3790–3798. [CrossRef]
24. Mir, A.; Chen, J.; Robinson, K.; Lendy, E.; Goodman, J.; Neau, D.; Golden, B.L. Two divalent metal ions and conformational changes play roles in the hammerhead ribozyme cleavage reaction. *Biochemistry* **2015**, *54*, 6369–6381. [CrossRef] [PubMed]
25. Mir, A.; Golden, B.L. Two active site divalent ions in the crystal structure of the hammerhead ribozyme bound to a transition state analogue. *Biochemistry* **2016**, *55*, 633–636. [CrossRef]
26. Kuimelis, R.G.; McLaughlin, L.W. *Nucleic Acids and Molecular Biology*; Eckstein, F., Lilley, D.M.J., Eds.; Springer: Berlin/Heidelberg, Germany, 1996; Volume 10, pp. 197–215.
27. Han, J.; Burke, J.M. Model for General Acid-base catalysis by the hammerhead ribozyme: pH-activity relationships of G8 and G12 variants at the putative active site. *Biochemistry* **2005**, *44*, 7864–7870. [CrossRef]
28. Nelson, J.A.; Uhlenbeck, O.C. Hammerhead redux: Does the new structure fit the old biochemical data? *RNA* **2008**, *14*, 605–615. [CrossRef]
29. Nelson, J.A.; Uhlenbeck, O.C. Minimal and extended hammerheads utilize a similar dynamic reaction mechanism for catalysis. *RNA* **2008**, *14*, 43–54. [CrossRef]
30. Thomas, J.M.; Perrin, D.M. Probing general base catalysis in the hammerhead ribozyme. *J. Am. Chem. Soc.* **2008**, *130*, 15467–15475. [CrossRef]
31. Frankel, E.A.; Strulson, C.A.; Keating, C.D.; Bevilacqua, P.C. Cooperative interactions in the hammerhead ribozyme drive pK_a shifting of G12 and its stacked base C17. *Biochemistry* **2017**, *56*, 2537–2548. [CrossRef]
32. Lilley, D.M.J. Classification of the nucleolytic ribozymes based upon catalytic mechanism. *F1000Research* **2019**, *8*, 1462. [CrossRef] [PubMed]
33. Hattori, Y.; Yamanaka, D.; Morioka, S.; Yamaguchi, T.; Tomonari, H.; Kojima, C.; Tanaka, Y. NMR spectroscopic characterization of a model RNA duplex reflecting the core sequence of hammerhead ribozymes. *Nucleosides Nucleotides Nucleic Acids* **2018**, *37*, 383–396. [CrossRef] [PubMed]
34. Pley, H.W.; Flaherty, K.M.; McKay, D.B. Three-dimensional structure of a hammerhead ribozyme. *Nature* **1994**, *372*, 68–74. [CrossRef] [PubMed]
35. Scott, W.G.; Murray, J.B.; Arnold, J.R.; Stoddard, B.L.; Klug, A. Capturing the structure of a catalytic RNA intermediate: The hammerhead ribozyme. *Science* **1996**, *274*, 2065–2069. [CrossRef]
36. Baeyens, K.J.; De Bondt, H.L.; Pardi, A.; Holbrook, S.R. A curved RNA helix incorporating an internal loop with G·A and A·A non-Watson–Crick base pairing. *Proc. Natl. Acad. Sci. USA* **1996**, *93*, 12851–12855. [CrossRef]
37. Tanaka, Y.; Morita, E.H.; Hayashi, H.; Kasai, Y.; Tanaka, T.; Taira, K. Well-conserved tandem G-A pairs and the flanking C-G pair in hammerhead ribozymes are sufficient for capture of structurally and catalytically important metal ions. *J. Am. Chem. Soc.* **2000**, *122*, 11303–11310. [CrossRef]
38. Tanaka, Y.; Kojima, C.; Morita, E.H.; Kasai, Y.; Yamasaki, K.; Ono, A.; Kainosho, M.; Taira, K. Identification of the metal ion binding site on an RNA motif from hammerhead ribozyme using ^{15}N NMR spectroscopy. *J. Am. Chem. Soc.* **2002**, *124*, 4595–4601. [CrossRef]

39. Tanaka, Y.; Kasai, Y.; Mochizuki, S.; Wakisaka, A.; Morita, E.H.; Kojima, C.; Toyozawa, A.; Kondo, Y.; Taki, M.; Takagi, Y.; et al. Nature of the chemical bond formed with the structural metal ion at the A9/G10.1 motif derived from hammerhead ribozymes. *J. Am. Chem. Soc.* **2004**, *126*, 744–752. [CrossRef]
40. Wang, G.; Gaffney, B.L.; Jones, R.A. Differential Binding of Mg^{2+}, Zn^{2+}, and Cd^{2+} at two sites in a hammerhead ribozyme motif, determined by ^{15}N NMR. *J. Am. Chem. Soc.* **2004**, *126*, 8908–8909. [CrossRef]
41. Liu, H.; Yu, X.; Chen, Y.; Zhang, J.; Wu, B.; Zheng, L.; Haruehanroengra, P.; Wang, R.; Li, S.; Lin, J.; et al. Crystal structure of an RNA-cleaving DNAzyme. *Nat. Commun.* **2017**, *8*, 2006. [CrossRef]
42. Cepeda-Plaza, M.; McGhee, C.E.; Lu, Y. Evidence of a general acid-base catalysis mechanism in the 8-17 DNAzyme. *Biochemistry* **2018**, *57*, 1517–1522. [CrossRef] [PubMed]
43. Velikyan, I.; Acharya, S.; Trifonova, A.; Földesi, A.; Chattopadhyaya, J. The pK_a's of 2′-hydroxyl group in nucleosides and nucleotides. *J. Am. Chem. Soc.* **2001**, *123*, 2893–2894. [CrossRef] [PubMed]
44. Acharya, S.; Acharya, P.; Földesi, A.; Chattopadhyaya, J. Cross-Modulation of Physicochemical Character of Aglycones in Dinucleoside (3′→5′) Monophosphates by the Nearest Neighbor Interaction in the Stacked State. *J. Am. Chem. Soc.* **2002**, *124*, 13722–13730. [CrossRef] [PubMed]
45. Lupták, A.; Ferré-D'Amaré, A.R.; Zhou, K.; Zilm, K.W.; Doudna, J.A. Direct pK_a measurement of the active-site cytosine in a genomic hepatitis delta virus ribozyme. *J. Am. Chem. Soc.* **2001**, *123*, 8447–8452. [CrossRef]
46. Guo, M.; Spitale, R.C.; Volpini, R.; Krucinska, J.; Cristalli, G.; Carey, P.R.; Wedekind, J.E. Direct Raman measurement of an elevated base pK_a in the active site of a small ribozyme in a precatalytic conformation. *J. Am. Chem. Soc.* **2009**, *131*, 12908–12909. [CrossRef]
47. Liu, L.; Cottrell, J.W.; Scott, L.G.; Fedor, M.J. Direct measurement of the ionization state of an essential guanine in the hairpin ribozyme. *Nat. Chem. Biol.* **2009**, *5*, 351–357. [CrossRef]
48. Liberman, J.A.; Guo, M.; Jenkins, J.L.; Krucinska, J.; Chen, Y.; Carey, P.R.; Wedekind, J.E. A transition-state interaction shifts nucleobase ionization toward neutrality to facilitate small ribozyme catalysis. *J. Am. Chem. Soc.* **2012**, *134*, 16933–16936. [CrossRef]
49. Dawson, R.M.C.; Elliott, D.C.; Elliott, W.H.; Jones, K.M. *Data for Biochemical Research*, 5th ed.; Clarendon Press: Oxford, UK, 1959; Chapter 5; p. 109.
50. Murray, J.B.; Seyhan, A.A.; Walter, N.G.; Burke, J.M.; Scott, W.G. The hammerhead, hairpin and vs. ribozymes are catalytically proficient in monovalent cations alone. *Chem. Biol.* **1998**, *5*, 587–595. [CrossRef]
51. Roychowdhury-Saha, M.; Burke, D.H. Distinct reaction pathway promoted by non-divalent-metal cations in a tertiary stabilized hammerhead ribozyme. *RNA* **2007**, *13*, 841–848. [CrossRef]
52. Boots, J.L.; Canny, M.D.; Azimi, E.; Pardi, A. Metal ion specificities for folding and cleavage activity in the Schistosoma hammerhead ribozyme. *RNA* **2008**, *14*, 2212–2222. [CrossRef]
53. O'Rear, J.L.; Wang, S.; Feig, A.L.; Beigelman, L.; Uhlenbeck, O.C.; Herschlag, D. Comparison of the hammerhead cleavage reactions stimulated by monovalent and divalent cations. *RNA* **2001**, *7*, 537–545. [CrossRef]
54. Takagi, Y.; Inoue, A.; Taira, K. Analysis on a cooperative pathway involving multiple cations in hammerhead reactions. *J. Am. Chem. Soc.* **2004**, *126*, 12856–12864. [CrossRef] [PubMed]
55. Wang, S.; Karbstein, K.; Peracchi, A.; Beigelman, L.; Herschlag, D. Identification of the hammerhead ribozyme metal ion binding site responsible for rescue of the deleterious effect of a cleavage site phosphorothioate. *Biochemistry.* **1999**, *38*, 14363–14378. [CrossRef] [PubMed]
56. Yoshinari, K.; Taira, K. A further investigation and reappraisal of the thio effect in the cleavage reaction catalyzed by a hammerhead ribozyme. *Nucleic Acids Res.* **2000**, *28*, 1730–1742. [CrossRef] [PubMed]
57. Katahira, M.; Kanagawa, M.; Sato, H.; Uesugi, S.; Fujii, S.; Kohno, T.; Maeda, T. Formation of sheared G:A base pairs in an RNA duplex modelled after ribozymes, as revealed by NMR. *Nucleic Acids Res.* **1994**, *22*, 2752–2759. [CrossRef]
58. Zhou, D.M.; Taira, K. The hydrolysis of RNA: From theoretical calculations to the hammerhead ribozyme-mediated cleavage of RNA. *Chem. Rev.* **1998**, *98*, 991–1026. [CrossRef]
59. Zhou, D.M.; He, Q.C.; Zhou, J.M.; Taira, K. Explanation by a putative triester-like mechanism for the thio effects and Mn^{2+} rescues in reactions catalyzed by a hammerhead ribozyme. *FEBS Lett.* **1998**, *431*, 154–160. [CrossRef]
60. Loverix, S.; Winqvist, A.; Strömberg, R.; Steyaert, J. Mechanism of RNase T1: Concerted triester-like phosphoryl transfer via a catalytic three-centered hydrogen bond. *Chem. Biol.* **2000**, *7*, 651–658. [CrossRef]
61. Kuzmin, Y.I.; Da Costa, C.P.; Fedor, M.J. Role of an active site guanine in hairpin ribozyme catalysis probed by exogenous nucleobase rescue. *J. Mol. Biol.* **2004**, *340*, 233–251. [CrossRef]
62. Ward, W.L.; DeRose, V.J. Ground-state coordination of a catalytic metal to the scissile phosphate of a tertiary-stabilized hammerhead ribozyme. *RNA* **2012**, *18*, 16–23. [CrossRef]
63. Lopez, X.; Schaefer, M.; Dejaegere, A.; Karplus, M. Theoretical evaluation of pK_a in phosphoranes: Implications for phosphate ester hydrolysis. *J. Am. Chem. Soc.* **2002**, *124*, 5010–5018. [CrossRef] [PubMed]
64. Mlýnský, V.; Banáš, P.; Walter, N.G.; Šponer, J.; Otyepka, M. QM/MM studies of hairpin ribozyme self-cleavage suggest the feasibility of multiple competing reaction mechanisms. *J. Phys. Chem. B* **2011**, *115*, 13911–13924. [CrossRef] [PubMed]
65. Kasai, Y.; Tanaka, Y.; Morita, E.H.; Tanaka, Y.; Taira, K. Physicochemical analysis of the interaction between a metal ion and the metal-ion-binding motif in hammerhead ribozymes. *Nucleic Acids Res.* **2001**, (Suppl. S1), 81–82. [CrossRef]
66. Santa Lucia, J., Jr.; Turner, D.H. Structure of $(rGGCGAGCC)_2$ in solution from NMR and restrained molecular dynamics. *Biochemistry* **1993**, *32*, 12612–12623. [CrossRef] [PubMed]

67. Devlin, F.J.; Finley, J.W.; Stephens, P.J.; Frisch, M.J. Ab Initio Calculation of Vibrational Absorption and Circular Dichroism Spectra Using Density Functional Force Fields: A Comparison of Local, Nonlocal, and Hybrid Density Functionals. *J. Phys. Chem.* **1995**, *99*, 16883–16902. [CrossRef]
68. Vosko, S.H.; Wilk, L.; Nusair, M. Accurate spin-dependent electron liquid correlation energies for local spin density calculations: A critical analysis. *Can. J. Phys.* **1980**, *58*, 1200–1211. [CrossRef]
69. Lee, C.T.; Yang, W.T.; Parr, R.G. Development of the Colle-Salvetti correlation-energy formula into a functional of the electron density. *Phys. Rev. B Condens. Matter Mater. Phys.* **1988**, *37*, 785–789. [CrossRef]
70. Becke, A.D. Density-functional thermochemistry. III. The role of exact exchange. *J. Chem. Phys.* **1993**, *98*, 5648–5652. [CrossRef]
71. Harihara, P.C.; Pople, J.A. The influence of polarization functions on molecular-orbital hydrogenation energies. *Theor. Chim. Acta* **1973**, *28*, 213–222. [CrossRef]
72. Banks, J.L.; Beard, H.S.; Cao, Y.X.; Cho, A.E.; Damm, W.; Farid, R.; Felts, A.K.; Halgren, T.A.; Mainz, D.T.; Maple, J.R.; et al. Integrated Modeling Program, Applied Chemical Theory (IMPACT). *J. Comput. Chem.* **2005**, *26*, 1752–1780. [CrossRef]
73. Bochevarov, A.D.; Harder, E.; Hughes, T.F.; Greenwood, J.R.; Braden, D.A.; Philipp, D.M.; Rinaldo, D.; Halls, M.D.; Zhang, J.; Friesner, R.A. Jaguar: A high-performance quantum chemistry software program with strengths in life and materials sciences. *Int. J. Quantum Chem.* **2013**, *113*, 2110–2142. [CrossRef]
74. Friesner, R.A.; Guallar, V. Ab initio quantum chemical and mixed quantum mechanics/molecular mechanics (QM/MM) methods for studying enzymatic catalysis. *Annu. Rev. Phys. Chem.* **2005**, *56*, 389–427. [CrossRef] [PubMed]
75. Anderson, M.P.; Uvdal, P. New scale factors for harmonic vibrational frequencies using the B3LYP density functional method with the triple-zeta basis set 6-311+G(d,p). *J. Phys. Chem. A* **2005**, *109*, 2937–2941. [CrossRef] [PubMed]
76. Marenich, A.V.; Cramer, C.J.; Truhlar, D.G. Universal Solvation Model Based on Solute Electron Density and on a Continuum Model of the Solvent Defined by the Bulk Dielectric Constant and Atomic Surface Tensions. *J. Phys. Chem. B* **2009**, *113*, 6378–6396. [CrossRef]
77. Cheeseman, J.R.; Trucks, G.W.; Keith, T.A.; Frisch, M.J. A comparison of models for calculating nuclear magnetic resonance shielding tensors. *J. Chem. Phys.* **1996**, *104*, 5497–5509. [CrossRef]